










Unveiling the solution structure of a DNA duplex with continuous silver-modified Watson-Crick base pairs

Received: 21 December 2023

Accepted: 20 August 2024

Published online: 05 September 2024

 Check for updates

Uroš Javornik ^{1,2,8}, Antonio Pérez-Romero^{3,8}, Carmen López-Chamorro³, Rachele M. Smith⁴, José A. Dobado ⁵, Oscar Palacios ⁶, Mrinal K. Bera⁷, May Nyman ⁴ , Janez Plavec ^{1,2}  & Miguel A. Galindo ³ 

The challenge of transforming organized DNA structures into their metallized counterparts persists in the scientific field. In this context, utilizing DNA molecules modified with 7-deazapurine, provides a transformative solution. In this study, we present the solution structure of a DNA duplex that can be transformed into its metallized equivalent while retaining the natural base pairing arrangement through the creation of silver-modified Watson-Crick base pairs. Unlike previously documented X-ray structures, our research demonstrates the feasibility of preserving the intrinsic DNA self-assembly while incorporating Ag^I into the double helix, illustrating that the binding of silver does not disrupt the canonical base-pairing organization. Moreover, in our case, the uninterrupted Ag^I chain deviates from forming conventional straight linear chains; instead, it adheres to a helical arrangement dictated by the underlying DNA structure. This research challenges conventional assumptions and opens the door to precisely design structures based on the organization of highly stable Ag-DNA assemblies.

DNA, considered the essential molecule of life, has evolved into a versatile tool for cutting-edge science through the concept of DNA nanotechnology pioneered by Seeman¹. In this context, DNA functions as the molecular equivalent of LEGO blocks, with single-stranded DNA (ss-DNA) serving as basic building units. Researchers can ingeniously program these units to self-assemble into intricate, customized structures on the nanoscale^{2,3}, such as polyhedra⁴, lattices⁵, cages, nanomachines⁶, or origami⁷ while adhering to Watson–Crick (W-C) base pairing rules. This versatile methodology continues to captivate scientists across various disciplines, presenting them with the ambitious challenge of enhancing DNA assemblies with properties that go beyond the inherent characteristics of nucleic

acids, while preserving their designed shapes. Towards this purpose, the metallization of DNA molecules has been widely explored due to the unique intrinsic properties metals can provide^{8,9}. However, metallizing DNA for control at the nanoscale is a significant goal. The challenge lies in the non-specific binding of metal ions, leading to unpredictable complex metallic DNA assemblies. To address this, metal-mediated or -modified base pairs¹⁰ offer a solution, enabling precise control over metal positioning and stoichiometry^{11,12}. Although researchers have successfully created metal-DNA systems with individual metal ions in double helix structures, fully metallized DNA structures remain limited^{13–18}, and predicting their structure has been a challenge.

¹Slovenian NMR Center, National Institute of Chemistry, SI-1000 Ljubljana, Slovenia. ²Faculty of Chemistry and Chemical Technology, University of Ljubljana, SI-1000 Ljubljana, Slovenia. ³Departamento de Química Inorgánica, Universidad de Granada, 18001 Granada, Spain. ⁴Department of Chemistry, Oregon State University, Corvallis, OR 97331-4003, USA. ⁵Departamento de Química Orgánica, Universidad de Granada, 18001 Granada, Spain. ⁶Departament de Química, Universitat Autònoma de Barcelona, 08193 Cerdanyola del Vallès, Barcelona, Spain. ⁷NSF's ChemMatCARS, Pritzker School of Molecular Engineering, University of Chicago, Chicago, IL 60637, USA. ⁸These authors contributed equally: Uroš Javornik, Antonio Pérez-Romero.

 e-mail: may.nyman@oregonstate.edu; janez.plavec@ki.si; magalindo@ugr.es

In this context, we have developed a method to introduce Ag^I ions into oligonucleotides at each base pair. Our findings strongly indicate that this approach maintains the integrity of the canonical base pairing arrangement through W-C metal-modified base pairs^{15,16}. This is achieved using 7-deazaadenine (X) and 7-deazaguanine (Y) analogs in place of A and G bases, forming hydrogen-bonded X-T and Y-C base pairs^{19,20}. Upon introducing Ag^I ions, these transform into silver-modified X-Ag^I-T and Y-Ag^I-C base pairs that can maintain the original W-C structure. This methodology allows for the creation of ^{7d}DNA molecules and their conversion into silver-^{7d}DNA equivalent, where Ag^I ions replace hydrogen bonds. Unlike previous research, which lacked the preservation of the W-C arrangement, our method provides improved predictability and design control for metal-DNA duplex structures.

This work elucidated the solution-state structure of a silver-^{7d}DNA double helix containing entire silver-modified Watson-Crick base pairs. Our results demonstrated that ^{7d}DNA molecules can create predictable silver-^{7d}DNA-based assemblies by following canonical base pairing rules. We have employed a variety of different techniques, including circular dichroism (CD), mass spectrometry (ESI-HRMS), nuclear magnetic resonance (NMR) and UV-Vis spectroscopy, and small-angle x-ray scattering (SAXS) to reveal the interaction of Ag^I within the interior positions of a ^{7d}DNA molecule. Notably, the structural features of the resulting silver-^{7d}DNA system were determined using high-resolution NMR spectroscopy and density functional (DFT) calculations.

Results

Formation of silver-metalated base pairs

In our investigation, we employed the self-complementary oligonucleotide sequence 5'-d(YYX CTC YXY TCC)-3' (ODN1, forms duplex I), akin to the one utilized in previous research that reported the

consecutive formation of silver-metalized base pairs within the DNA double helix¹⁴. However, in this particular study, we introduced a modification by replacing the canonical A and G bases with 7-deazaadenine (X) and 7-deazaguanine (Y) bases, respectively. Additionally, we substituted the C base in the ninth position with the Y base to create a self-complementary C-Y base pair, in contrast to the C-C mismatch pair in the previous research. To facilitate a comparison with results obtained using ODN1, we employed the equivalent canonical sequence 5'-d(GGA CTC GAG TCC)-3' as a reference (ODN2, forms duplex II).

We conducted initial CD titration experiments to investigate conformational changes in duplexes I and II upon interaction with Ag^I ions. Both free duplexes displayed distinct CD features, with a maximum at 280 nm and a minimum at 245 nm (Fig. 1). For duplex I, the addition of Ag^I resulted in a gradual reduction in ellipticity and flattening of the 280 nm band, with changes stabilizing upon adding 1 equivalent of Ag^I per base pair (Ag/bp), thus indicating a saturation point (Fig. 1a). In contrast, duplex II showed a decrease in ellipticity and a complete inversion of the entire CD spectrum, manifesting a pronounced descending band at 280 nm, also stabilizing soon after adding 1Ag/bp (Fig. 1b). The results indicate that both duplexes interact with Ag^I ions but leading to different conformational changes. A comparative analysis of the CD spectra for duplex I and duplex I-Ag at 1Ag/bp suggests that these structures may share structural similarities. This conclusion arises from the observation that the CD profile of duplex I-Ag exhibits reduced ellipticity while maintaining a very similar profile to that of duplex I, with both spectra exhibiting a decline around 245 nm and an ascent around 280 nm, indicating closely superimposable profiles (Fig. 1c). These similarities highlight the close conformational relationship between duplex I and I-Ag. This assertion gains further support when examining the differences between canonical duplex II and II-Ag at the same point. In this case, the CD curves

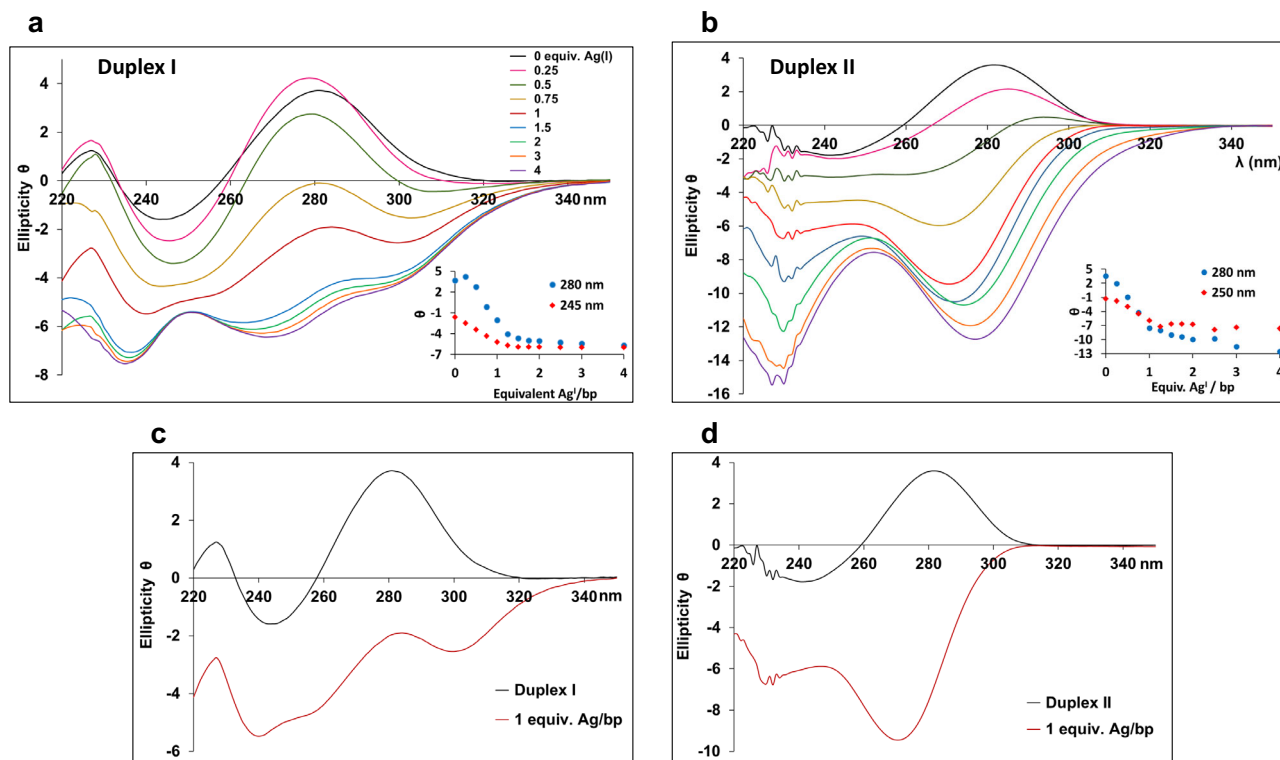


Fig. 1 | CD spectra in the absence and presence of Ag^I ions. a, b CD curves registered for duplex I and II, respectively, upon adding a controlled amount of Ag^I. **c, d** Ellipticity variation at the bands centered at 250 and 280 nm for duplex I and II,

respectively. Conditions: 2 μM duplex, 5 mM MOPS pH 8.5, 100 mM NaClO₄, Ag^I equivalent (equiv.) per base pair (bp) indicated in the inset.

exhibited complete inversion with respect to each other, resembling mirror images (Fig. 1d), indicating that the **II-Ag** adopted a completely new organization. According to previous studies on canonical sequences, this new organization arises through the formation of non-canonical metallated base pairs, where Ag-binding to purine N7-positions plays a key role^{13,21,22}. However, duplex **I-Ag** cannot form metallated base pairs involving the purines N7-atom, implying that its metalation process must involve the formation of alternative silver-metallized base pairs.

UV-variable temperature measurements were conducted to investigate the denaturation behavior of duplexes **I** and **II** in the presence and absence of Ag⁺ ions. In the absence of Ag⁺ ions, both duplex **I** and **II** exhibited sigmoidal melting curves with a melting temperature of 42 and 51 °C, respectively (Supplementary Fig. 1). The variation between them is attributable to the weaker hydrogen bonds formed by 7-deazapurine nucleobases in duplex **I**. The addition of Ag⁺ ions caused a gradual flattening of the melting curves during the titration experiment until they disappeared in the presence of 1Ag/bp. The primary conclusion derived from these findings is the formation of metallated species, where metal ions replace canonical hydrogen bonds, increasing the duplexes' thermal stability. This enhanced stability surpasses the experimental measurement range in the presence of 1Ag/bp. It is important to exercise caution if attempting to draw conclusions from the melting curves recorded before reaching the saturation point at 1Ag/bp. Before saturation and throughout the titration experiment, fully metallized duplexes coexist with mixed-partially or non-metallized duplexes (see NMR data discussion below), complicating the interpretation of the data. Therefore, we did not attempt to calculate the melting temperature variations, and our subsequent studies will be conducted at the saturation point to ensure more precise and reliable results.

To gain deeper insights into the denaturing process, we conducted CD-melting experiments for duplex **I** and **II** in the absence and presence of 1.1 equivalent of Ag⁺ per base pair, slightly exceeding the saturation point. In the absence of metal ions, the CD curves displayed a reversible behavior during the melting and alignment process, aligning with a denaturing reversible process (Supplementary Fig. 2). The ellipticity intensity variances of the CD curves at 20 °C before and after heating is attributed to condensation events occurring on the cuvette's surface, slightly altering the concentration without affecting CD curves shape. A plot of the CD variation with temperature showed the expected enhanced thermal stability for duplex **II** compared to duplex **I**, mirroring the results of the UV-melting experiment (Supplementary Fig. 2d, 2d'). However, in the presence of 1 equiv. of Ag⁺ ions, different outcomes were observed for each duplex. Duplex **I-Ag** experienced reversible changes during the heating-cooling process, whereas duplex **II-Ag** underwent a non-reversible conformational change. This difference is particularly evident when comparing the CD curves at 90 and 20 °C (after cooling), as **I-Ag** displayed markedly different CD profiles at the two temperatures, whereas **II-Ag** displayed similar curves (Supplementary Fig. 3d, 3d'). The CD and UV experiments clearly demonstrated that the binding of Ag⁺ to duplex **I** and **II** leads to more stable species. However, the resulting conformational changes were markedly different for each duplex. Since it is well-known that the purine N7-position plays a crucial role in stabilizing silver-metallized canonical duplexes, the absence of 7-deazapurines in duplex **II** could promote the formation of silver-modified Watson-Crick base pairs.

The electrospray ionization mass spectrometry (ESI-MS) experiment unequivocally provided evidence for the formation of **I-Ag** complex (Supplementary Fig. 4). The deconvoluted mass spectrum for the reaction between duplex **I** and Ag⁺ ions showed the peaks for duplex **I** (7281.0 g/mol) with 7-12 Ag⁺ ions (106.9 a.u) bound, demonstrating the formation of **I-Ag** complexes, including the saturated system with twelve metal ions (Supplementary Table 1).

SAXS and ASAXS studies of silver-DNA duplexes

Small-angle X-ray scattering (SAXS) and anomalous small-angle X-ray scattering (ASAXS) provided structural information about duplexes **I** and **II** in the absence and presence of Ag⁺ ions. The scattering data for duplex **I** (at 0.7 mM) is consistent with the formation of a double helix structure, exhibiting an excellent match with the simulated scattering, up to q value of 0.2 Å⁻¹ (Supplementary Fig. 5). Above this q value, the experimental curve starts to incorporate solvent scattering, primarily due to the relatively weak scattering of the low-concentration and light-atom species. Nonetheless, the match is convincing within the entire Guinier region (q -0.01 to 0.2 Å⁻¹), confirming the expected size and shape of the double helix (vide infra). Adding 1.1 equiv. Ag⁺ per base pair to duplex **I** leads to only small changes in the scattering data, suggesting the incorporation of Ag⁺ does not lead to significant conformational changes. We performed a PDDF (pair distance distribution function) analysis of the scattering data, which revealed the differences and similarities of the scattering, with and without Ag⁺ ions (Fig. 2 and Supplementary Figs. 6, 7). The PDDF is a probability distribution of scattering vectors through the dissolved species, obtained by a Fourier transform of the reciprocal space scattering data. The maximum diameter (r) where probability goes to 0 describes the maximum diameter of the scattering species; 37.4 Å for duplex **I** and 36.1 Å for **I-Ag**, precisely equivalent to the length of the duplex **I**. A slightly smaller R_g (radius of gyration, a shape independent, root mean square average of the distance of the electrons from the center of the particle) is reported for **I-Ag** than for duplex **I** (Supplementary Figs. 6, 7). This is consistent with the incorporation of the Ag⁺ ions in the center of the helix, more thoroughly evaluated with ASAXS, discussed below. The addition of Ag⁺ also increases the P(r), also due to the presence of heavy atoms in the center, and a low shoulder to the right appears (Fig. 2). The low shoulder indicates a bimodal electron density, with lower scattering intensity from the shell (the DNA surrounding the Ag-chain).

To determine the precise location of Ag⁺ within both the **I-Ag** and **II-Ag** complexes, we conducted ASAXS measurements at a synchrotron source. This involved collecting SAXS data using X-rays at 20 different energy levels, each situated just 1 keV below the silver K-edge at 25.514 keV (Supplementary Figs. 8–24, Supplementary Tables 2, 3 for **I-Ag**, and Table 4 for **II-Ag**). For this investigation, we performed detailed modeling of various scattering components based on the solid cylinder model for these complexes (Fig. 3a). A comparative analysis of the data revealed that both duplexes contained Ag⁺ within the cylindrical region, meaning the double helices encapsulate them. However, **I-Ag** saturates at approximately 1 equivalent and **II-Ag** does not reach saturation within our experimental range of 3 equivalents (Fig. 3b). The length of **I-Ag** structure remained relatively consistent at around 40 Å. In contrast, **II-Ag** structure substantially increased, indicative of polymerization events (Fig. 3c and Supplementary Table 4). Overall, the modeling data indicated that Ag⁺ interacts with the interior regions of the double helices in both **I-Ag** and **II-Ag** complexes but yielding different structural outcomes, as also revealed by the herein described CD experiments.

High-resolution NMR studies of silver-DNA duplexes

NMR spectroscopy measurements were employed to further study the interaction of Ag⁺ ions with duplex **I** and **II**. For this, a solution of duplex **I** was titrated with Ag⁺ in the range between 0 and 2.5Ag/bp. ¹H NMR spectra were recorded at various points during the titration to monitor the interaction (Fig. 4a). Based on signals corresponding to hydrogen-bonded imino (δ 12–15 ppm) and amino (δ 8–9 ppm) protons, the spectra indicate a double-stranded structure for the oligonucleotide at the start of titration. After adding Ag⁺ ions, the signals characteristic for the starting duplex structure began to decrease. Then, several new signals appeared in the spectra, indicating an interaction between duplex **I** and Ag⁺ ions. Finally, at about 1.5 equivalents, the signals converged into a single set, which stayed unchanged until the

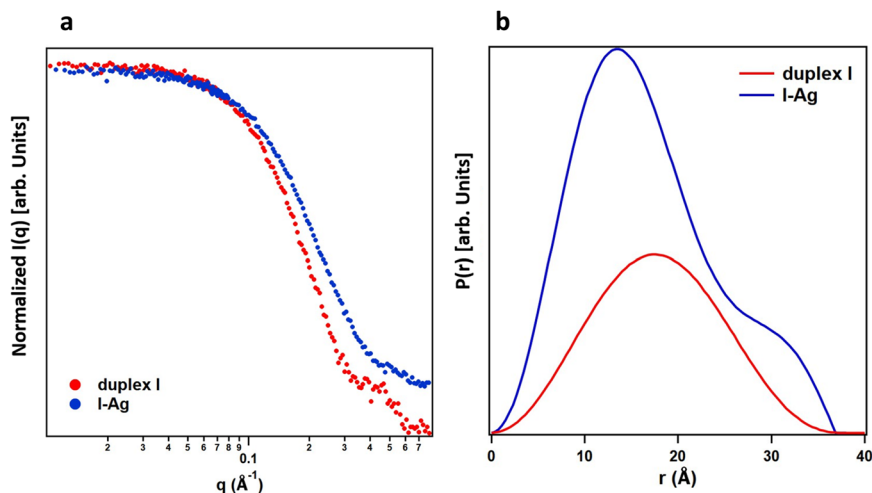


Fig. 2 | Scattering data from benchtop SAXS (Cu-K α radiation, 8.04 keV) of duplex I, in the absence and presence of 1.1 equivalent Ag/bp (I-Ag). **a scattering plot and **b** pair distance distribution function (PDDF) analysis.**

endpoint of the titration (Fig. 4a, b). The presence of four signals originating from amino protons indicates the formation of hydrogen bonds within the final structure. The number of non-exchangeable signals suits a symmetric antiparallel double-stranded structure similar to the one adopted natively by duplex I. Notably, the imino proton signals are absent in line with the expected position of the coordinated Ag^I ions in place of T-H3 and Y-H1 protons in the modified base pairs. The double-stranded nature of the final structure was further confirmed by DOSY NMR measurements, which gave similar translational diffusion coefficients (D_T) of 1.15 and $1.16 \cdot 10^{-10} \text{ m}^2 \text{ s}^{-1}$ for the Ag^I free and bound structures, respectively, under comparable conditions. This is also similar to the D_T measured for the canonical duplex II analog at $1.21 \cdot 10^{-10} \text{ m}^2 \text{ s}^{-1}$, indicating a comparable hydrodynamic radius for all three structures.

The appearance of additional signals in ¹H NMR spectra during the titration with Ag^I indicates that the incorporation of silver proceeds through several partially metallated intermediates with silver ions bound at various positions within the duplex. The presence of these intermediates is consistent with minor structural rearrangements associated with the incorporation of silver ions that permit the coexistence of silver-mediated and canonical base pairs. On the other hand, it has been observed previously that single-step transitions are typical where larger structure rearrangements, like base bulging or strand slipping, are required^{13,14}.

The entire process described for duplex I is in marked contrast to titration of the standard analog duplex II, where the number of signals in ¹H NMR spectra increased throughout the course of titration and did not converge to a single well-defined structure by ten equivalents Ag^I ions per base pair (Supplementary Fig. 28). These results are consistent with previous observations that Ag^I ions tend to promote the formation of non-canonical base pairs in DNA, such as C-Ag^I-C, T-Ag^I-T, or G-Ag^I-G homodimers, while the standard metallated Watson-Crick A-T and G-C are disfavored, leading to loss of base pairing pattern, emergence of an ensemble of structures with degenerate folding energies, and ultimately the aggregation of the refolded oligonucleotides^{13,14,21}. This is reflected by the progressive line broadening and signal loss in ¹H NMR spectra with increasing concentrations of silver ions in the solution.

NMR reveals the structural characteristics of duplex Ag^I-DNA

A NOESY walk was completed in the aromatic-anomeric and the aromatic-H2'/H2'' region for the entire length of the I-Ag complex (Fig. 4b), which is consistent with a right-handed double-helical structure with all χ torsion angles in *anti*-orientation. Cross peaks

involving protons of the Y7 residue were weaker than expected, indicating a possible distortion, or increased structural flexibility in the I-Ag complex at the C6-Y7 step.

H1'-H2' and H1'-H2'' cross-peak patterns in DQF-COSY spectra indicate South sugar pucker for most residues, except for C4, T10, C11, and C12, where higher ³J_{H1'H2''} values indicate a significant fraction of North sugar pucker for the respective ribose moieties. The same observation is true for duplex I and I-Ag and is a known feature of pyrimidine residues in general (Fig. 4b, c).

³¹P NMR chemical shifts for duplex I are similar to the canonical analog II in the absence of Ag^I ions. After the formation of the complex, the chemical shift of X3P, X8P and Y9P shift upfield by 0.5 to 1.1 ppm (Supplementary Fig. 29). This observation indicates a backbone rearrangement from the canonical BI type toward BII type. On the other hand, patterns in HP-COSY spectra mainly indicate similar H3' and H5'/H5'' J coupling values, which imply similar γ and β torsion angles for duplex I in the presence and absence of Ag^I ions, except for the C6-Y7 step, where the C6H3' to Y7P cross-peak is changed upon addition of the silver ions. This could be due to a backbone distortion at this step or due to the signal broadening observed for the Y7 residue.

We applied NMR restraints derived from NOESY and DQF-COSY spectra to construct structural models of the I and I-Ag duplexes in AMBER. The silver-modified model was constructed by replacing imino protons within Watson-Crick base pairs with silver ions. The appropriate parameters for the metal ion binding terms were determined based on DFT calculations in Gaussian software, and parameters for the metal-mediated base pairs were obtained with the help of MCPB software²³. A total of 250 NOE-derived distance restraints were applied for the native structure of duplex I and 320 for the silver-mediated duplex I-Ag structure. Additionally, sugar pucker was restrained to 140–180° range for residues 1-3 and 5-9 in both structures and backbone torsions were restrained in duplex I based on ³¹P NMR chemical shifts and HP-COSY cross-peaks.

The NMR structure shows duplex I-Ag forms a right-handed helical structure resembling the B-type DNA helix (Fig. 5a), with an average twist of 34° and an average rise of 3.3 Å (compared to 33° and 3.3 Å in the structure of duplex I, Supplementary Table 5). The main difference compared to the canonical structure is the reorientation of the bases required to accommodate the silver ions within the base pairs (Fig. 5b). The average base opening parameter for the silver-modified duplex is -35°, compared to values in the structure of duplex I without the silver ions (the latter is also the same as in a model B-type duplex). The propeller twist of the base pairs is also increased to an average value of -20°, compared to -8° in the model of duplex I or -11°

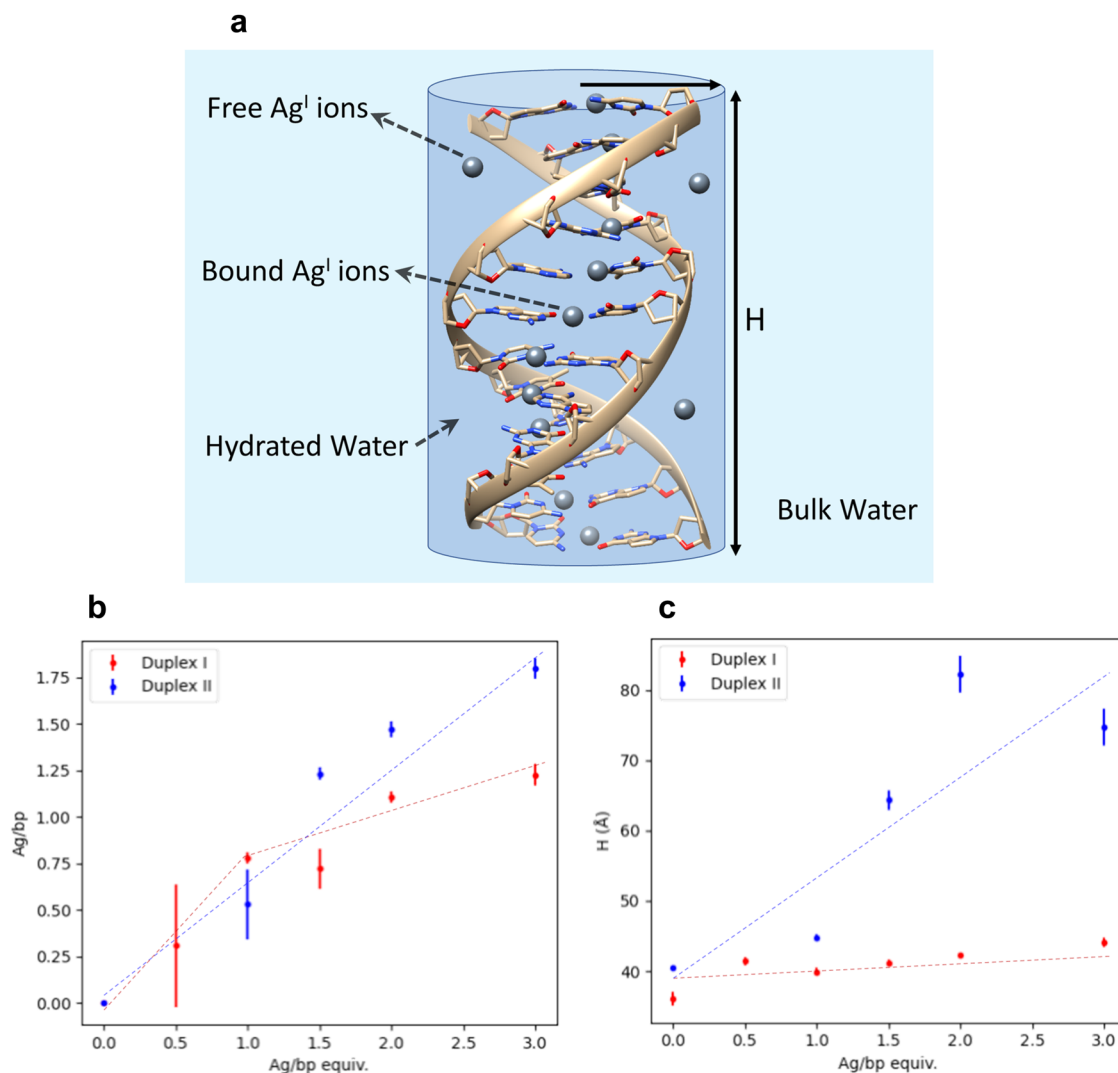


Fig. 3 | ASAXS modeling and analysis using a solid cylinder model of I-Ag and II-Ag complexes. **a** Solid cylinder model of the Ag-DNA complexes. The Ag⁺ ions can bind the base pairs or be free within the cylindrical regions. Metrical information derived from the Ag-DNA complexes modeling, namely: **b** the number of Ag⁺ per

base pairs of the complex (Ag/bp); **c** the lengths (H). The data were represented using red symbols with error bars for **I-Ag** complexes and blue symbols with error bars for **II-Ag** complexes, along with auxiliary lines to highlight the trend of the points.

for B-DNA type structures in general (Fig. 5c). The change in base pair geometry forces the breaking of one of the hydrogen bonds in the C-Y base pair, leaving the base pair connected with one hydrogen bond and the silver coordination bond in place of the original three hydrogen bonds. Our model suggests that the 2-amino groups of Y residues, which are released from hydrogen bonding in C-Y base pairs, tend to form inter-base pair hydrogen bonds when a purine residue precedes the residue. Four such pairs are observed in our model: Y2-C12*, T5-Y9*, Y9-T5*, and C12-Y2* (asterisks denote complementary strand residues). Inter-planar hydrogen bonding has been observed in silver ion-mediated DNA structures before and has been proposed as an important factor for structure stabilization¹⁴. The differences observed between C-Y and T-X base pairs, and between different base steps, could have implications for the stability of various sequences of the 7^dDNA system. Likewise, this structural detail could factor into the reasons why A-T base pairs have not been observed in native sequence contexts to date, while G-C pairs have.

The silver ions within duplex **I-Ag** form a helical arrangement mirroring the pattern of base pairs. The overall helix retains a narrow central cavity similar to the native B-type helix, and the silver ions

thread among the DNA bases, appearing obscured by the nucleobases when viewed from the top (Fig. 5a). The average distance between consecutive Ag⁺ ions along the structure is $3.8 \pm 0.3 \text{ \AA}$, exceeding the sum of the ionic radii (3.44 \AA), suggesting a general absence of argentophilic interactions²⁴. However, the distances between silver ions (Ag-Ag) vary depending on the sequence, reducing to 3.27 \AA at steps 3 and 9. This proximity seems primarily influenced by base pair shift, slide and atom distance within the base pairs and reflects the leading role of interactions between the DNA nucleotides in determining the position of silver ions. This observation suggests the possibility of directing potential electronic properties of the assemblies throughout DNA sequence. Notably, the Ag⁺ arrangement differs from that seen in previously published X-ray structures of silver-mediated structures of canonical DNA^{13,14}. This could reflect differences in the relative contribution of argentophilic interactions to the structures due to differences in nucleotide chemistry of applied conditions. A previously published solution structure of a DNA duplex with three consecutive silver-mediated base pairs did not show significant argentophilic interactions, similar to our findings here²⁵.

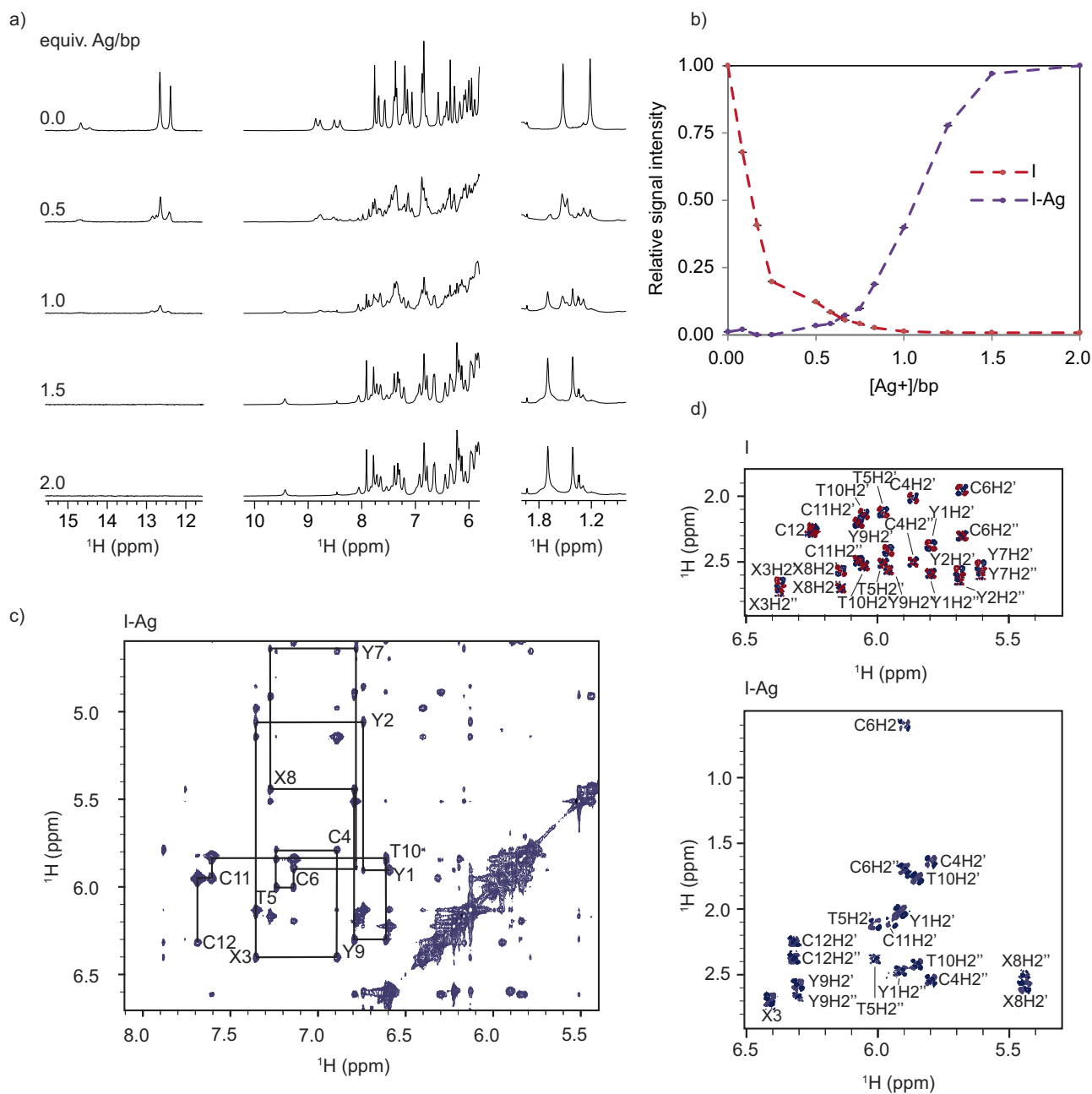


Fig. 4 | NMR spectra of the I/I-Ag system. a Alimino, aromatic, and methyl regions of ^1H NMR spectra of the titration, Ag^+ concentration presented in equivalents per base pair. **b** Normalized signal intensities of T10 H7 proton (methyl group) in **I** and **I-Ag**

structures in ^1H NMR spectra of the titration. **c** Aromatic-anomeric region of NOESY spectrum of **I-Ag** at 25°C showing the characteristic sequence walk. **d** $\text{H}1\text{-H}2'/\text{H}2''$ DQF-COSY spectra of **I** and **I-Ag** showing patterns characteristic of S sugar puckers.

DFT calculations verified the structure of I-Ag complex

To study the positioning of the Ag^+ ions more precisely, we performed DFT-based (PBEh-3c) calculations on the **I-Ag** complex in the presence of sodium counterions and water molecules. To our knowledge, no comprehensive DFT study has been conducted on an entire metal-DNA system with twelve consecutive metal-modified base pairs. Previous theoretical DFT (M06-2X) investigations in this area have been limited to fragments of up to six units in size²¹.

Notably, the DFT-optimized geometry of the **I-Ag** complex closely resembles the structure derived from the NMR data (Fig. 6 and Supplementary Table 5). These structures align in several critical aspects, suggesting a robust agreement between the two structure determination methods. While subtle differences in specific parameters exist, these distinctions do not reduce the broader concordance between

the NMR and DFT-optimized structure. For instance, the twist angle is approximately 34° in the NMR and DFT structures, showcasing a high level of agreement. Furthermore, parameters like the minor groove width, slide, rise, and tilt exhibit noteworthy alignment.

In addition, the parameters of buckle, opening, and major groove width appear to show minor variations considering the standard errors. However, the propeller angle ($-8^\circ \pm 9$) appears to be more distinct from that revealed in the NMR ($-21^\circ \pm 4$). It is essential to recognize that these differences are subtle and fall well within the range of experimental computational approximations. Thus, they do not detract from the overarching consensus on the core helical NMR structure of **I-Ag**.

Similar to the NMR-derived model, the Watson-Crick pairing is preserved, with silver ions substituting a hydrogen bond with a linear

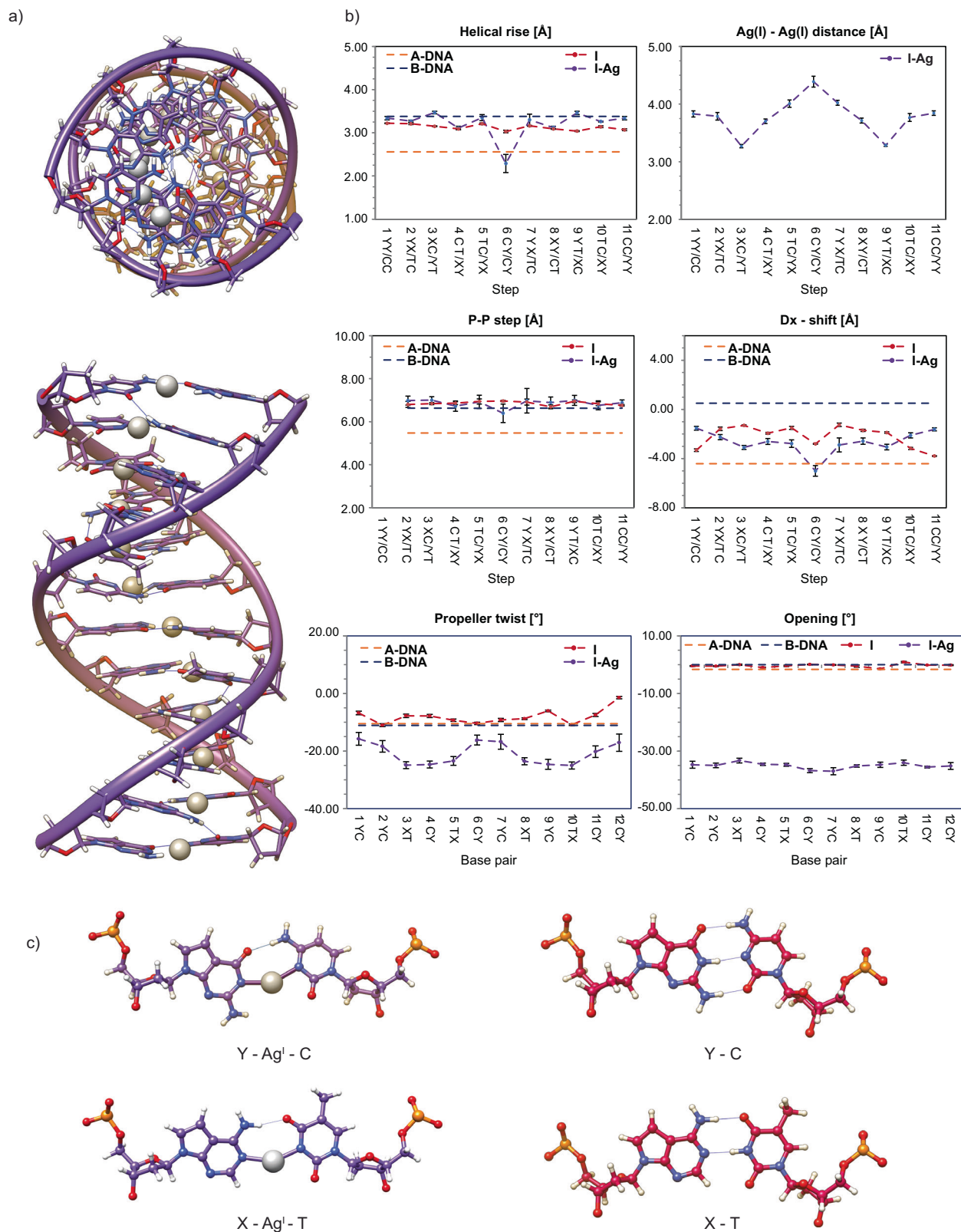


Fig. 5 | NMR structure of I-Ag complex and structural parameters for the duplex I and I-Ag complex. a Side and top views of the lowest energy structure following NMR restrained MD. **b** Selected structural parameters for I and I-Ag. While most structural parameters remain similar, the base pairs are perturbed, as

reflected in the propeller twist and base pair opening. Typical values for B-DNA and A-DNA type structures are indicated in the graphs, where applicable. **c** Base pair geometry for the metal-modified base pairs in I-Ag complex and duplex I.

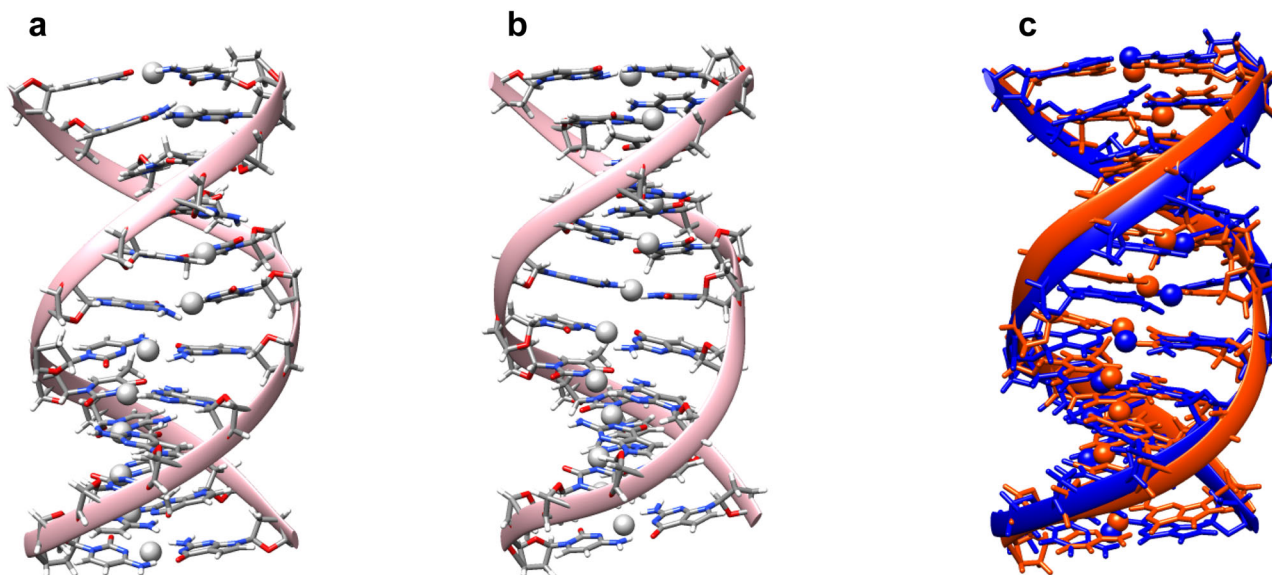


Fig. 6 | NMR vs. DFT Structural Comparison. Structures for **I-Ag** complex obtained by different methodologies: **a** NMR spectroscopy and **b** DFT calculations. **c** Superposition of the NMR (blue) and DFT (orange) structures.

coordination bond. These ions align according to the helix turn dictated by the base pairs, with an average $\text{Ag}\cdots\text{Ag}$ distance of $3.6 \pm 0.3 \text{ \AA}$, slightly smaller than observed in the NMR model (Supplementary Table 6). This situation excludes the formation of contiguous argentophilic interactions, confining them to specific regions throughout the sequence, particularly at steps 2, 3, and 9, in close accordance with the NMR data. This stands in contrast to the observations made in crystal structures of Ag -DNA systems featuring non-canonical base pairings, where a continuous array of argentophilic interactions occurs^{13,14}. However, in some sections of the double strand, certain silver ions are observed with distances less than 3.44 \AA , suggesting the potential existence of argentophilic interactions.

Discussion

The findings outlined in this study illustrate the potential of utilizing ^{7d}DNA molecules for constructing double helices made of silver-modified Watson-Crick pairing, as illustrated by the NMR solution structure of duplex **I-Ag**. A significant breakthrough emerges from the fact that **I-Ag** retains the original conformation of duplex **I**, initially formed by canonical Watson-Crick base pairs. Importantly, our study also revealed that the structural framework of duplex **I** dictate the helical organization of silver ions along the central axis, in contrast to prior X-ray diffraction findings. These exciting findings open the door for precisely engineering silver patterns at the nanoscale by strategically designing ^{7d}DNA molecules, and offering enhanced stability to programmed DNA-based nanostructures, leveraging canonical DNA assembly capabilities.

Methods

Oligonucleotide synthesis

The oligonucleotide ODN1 was synthesized with a K&A Laborgeraete GbR DNA/RNA synthesizer following manufacturer protocols. The non-canonical 7-deazaadenine and 7-deazaguanine phosphoramidites nucleosides were purchased from ChemBiotech (Münster, Germany) and Glen Research (Maravai LifeSciences, USA). The purification was performed by RP-HPLC using an Azura preparative 2.1L HPLC system (Knauer, Berlin, Germany) with a C18 column (Kromasyl EternityXT-5-C18), and acetonitrile/tetraethylammonium acetate buffer mobile phases. DMT groups were removed by reaction in 80% acetic acid for

30 min. Samples were then transferred to a pure water phase by ethyl ether extraction and desalted on a Sephadex G25 column using FPLC (ÄKTApurifier 10, GE HealthCare, Chicago, Illinois, USA). Desalted samples were lyophilized for further use and analyzed by HPLC (Supplementary Fig. 30). The oligonucleotide ODN2 was purchased from Sigma-Aldrich with HPLC purification grade. ESI-MS spectrometry (negative mode): Calcd for ODN1 [(C₁₂₂H₁₅₃N₄₀O₇₀P₁₁)-H]⁻: 3639.4496 Da, found: 3639.2654 Da (Supplementary Fig. 31). Calcd for ODN2 [C₁₁₆H₁₄₇N₄₆O₇₀P₁₁)-H]⁻: 3645.3773 Da, found: 3645.5057 Da (Supplementary Fig. 32).

UV-vis thermal spectroscopy

UV-vis spectra were recorded on an Agilent Technologies Cary 100 Spectrophotometer in association with a Temperature Controller. UV-melting curves were registered at 265 nm with a heating rate of $0.5 \text{ }^\circ\text{C}\cdot\text{min}^{-1}$ and data interval of $1 \text{ }^\circ\text{C}$. The melting curve graphs were prepared using normalized Absorbance ($A_{\text{norm}} = (A - A_{\text{min}})/(A_{\text{max}} - A_{\text{min}})$) at 265 nm.

CD spectroscopy

CD spectra were recorded on a Jasco J-815 instrument equipped with a Peltier temperature controller. The duplex **I** and **II** titration experiments upon adding controlled amounts of Ag^+ ions were recorded by keeping the corresponding duplex concentration constant at $2 \text{ }\mu\text{M}$ in water containing 100 mM NaClO_4 and 5 mM MOPS buffer at pH 8.5. The aliquots from a stock solution of AgClO_4 ($1000 \text{ }\mu\text{M}$) were added to this solution, along with identical aliquots from an oligonucleotide stock solution ($4 \text{ }\mu\text{M}$ DNA, 200 mM NaClO_4 , 10 mM MOPS buffer) to keep the DNA and buffer concentration constant.

ESI-MS spectrometry for silver-DNA complex

Molecular mass determination for **I-Ag** complexes was performed by ESI-MS using a Micro ToF-Q Instrument (Bruker Daltonics GmbH, Bremen, Germany) equipped with a time-of-flight analyzer (ESI-TOF MS), with ESI-L Low-Concentration Tuning Mix (Agilent Technologies, USA), interfaced with an Agilent Technologies Series 1100 HPLC pump and equipped with an autosampler, both controlled by the Compass Software. The interaction of duplex **I** (0.2 mM) with Ag^+ ions was analyzed in negative mode. For each experiment, $10\text{--}20 \text{ }\mu\text{L}$ of the sample was injected at $30\text{--}55 \text{ }\mu\text{L}\cdot\text{min}^{-1}$; the capillary counter

electrode voltage was 4.5 kV; desolvation temperature at 85 °C; dry gas at 6 L · min⁻¹. Spectra were collected throughout an m/z range from 500 to 2500. The liquid carrier was a 90:10 mixture of 25 mM ammonium acetate and acetonitrile, pH 7.5. Molecular mass determination for ODN1 and ODN2 were registered for 50 μM sample in Tris buffer, using a High-Resolution QTOF Mass Spectrometer (Bruker, Compact model) (Acquisition parameters shown in Supplementary Figs. 31, 32).

SAXS and ASAXS measurements

For these experiments, the duplexes were prepared at different concentrations. The concentrated samples (0.7 mM duplex) provided sufficient signal-to-noise dispersion data on the benchtop instrument (Anton Paar SAXSpace). On the other hand, more diluted samples (0.2 mM duplex) were employed to register scattering and anomalous scattering (ASAXS) data in a synchrotron source (Advanced Photon Source, APS).

X-ray scattering data were collected on an Anton Paar SAXSpace instrument equipped with a Cu-K α radiation source (1.54 Å) with line collimation, a Dectris Mythen 1K detector and a temperature-controlled sample stage (TCS150) with a capillary holder. Data was collected with the maximum sample-detector distance in high-intensity mode resulting in a $q = 0.01\text{--}0.78 \text{ \AA}^{-1}$ range. Samples were prepared in 1.5 mm borosilicate capillaries and sealed with paraffin wax. The sample temperature was lowered to 10 °C and held at this temperature for 5 min prior to data collection. Sample stability was monitored by collecting 3 × 15 min frames using Anton Paar's SAXS data software. If stable, these frames were averaged and processed using SAXSanalysis software (normalization, primary beam removal, background subtraction, and desmearing). All analyses and curve-fitting were carried out utilizing IRENA macros with IgorPro 6.3 (Wavemetrics) software²⁶. To simulate scattering data from the crystal structure, we used SolX software²⁷.

ASAXS data were collected for duplexes **I** and **II** at 0.2 mM concentration, with and without added Ag^I, over twenty energies from the Ag K-edge (25.5140 keV) to below the K-edge (24.5140 keV) at the NSF's ChemMatCARS (15-ID-D) beamline of Advanced Photon Source (APS). By utilizing the energy-dependent SAXS data, we extracted various scattering components, specifically the SAXS-terms, Cross-terms, and Resonant-terms (Supplementary Figs. 25, 26). The Resonant-terms of the scattered intensity provided valuable insight into the distribution of the Ag^I within the samples. However, due to the overall low-electron density contrast between the oligonucleotides and water, scattering from water dominated beyond 0.35 Å⁻¹. This dominance limited the resolution for locating ions within the complexes and therefore it was only feasible to model the complexes assuming a solid cylinder. The energy-dependent SAXS data were analyzed using a solid cylinder model to obtain information about the structure of the Ag-DNA complexes. The analysis details are available in the Supplementary Information in the AXSAX Analysis section.

NMR spectroscopy

NMR spectra were acquired on Bruker AVANCE NEO 600 and 800 MHz spectrometers equipped with QCI and TCI cryogenic probes at 25 °C, if not stated differently. NMR samples were prepared from DNA stock solutions at final 0.8 mM DNA oligonucleotide concentrations in 90%/10% H₂O/²H₂O or 100% ²H₂O, 100 mM NaClO₄, 100 mM Tris/HNO₃ (pH 8.6). Water suppression in ¹H and 2D ¹H-¹H NOESY ($\tau_m = 100$ ms) experiments was achieved by using excitation sculpting method. 2D ¹H-¹H TOCSY ($\tau_m = 80$ ms) and DQF-COSY spectra were acquired in 100% ²H₂O. Sixteen different gradient strengths (1-51 G·cm⁻¹) were used in DOSY experiments. ¹H NMR chemical shifts were referenced with respect to the signal at δ 0.0 ppm for external standard DSS. NMR spectra were processed and analyzed by using TopSpin (Bruker) and Sparky (UCSF) software.

Restraints. Distance restraints were obtained by integration of signals in NOE spectra. For non-exchangable signals, cytosine H5-H6 signals were used as a reference for distance (2.34 Å). For well-resolved and well-formed peaks, restraints were set as $d \pm 20\%$, while for partially overlapped, weak or malformed peaks, qualitative restraints were set based on binning to strong (1.8-3.6 Å), medium (2.6-5.0 Å) or weak (3.5-6.5 Å) classes. Hydrogen bonding restraints were set as upper bounds based on the standard Sanger geometries for duplex **I**. Hydrogen bond restraints for the silver-modified duplex **I-Ag** were set at 2.4 Å for the remaining hydrogen bond pairs (X H2 - T O2 and C H4 - Y O6) to account for the weaker or absent signals observed in the NMR spectra. Torsion restraints were included, which were set according to cross-peak patterns in DQF-COSY and HP-COSY spectra. Backbone torsions were restrained to a standard B-DNA type for duplex **I** based on ³¹P NMR chemical shifts and cross-peaks in ¹H-³¹P HP-COSY spectra (the following restraints were used: α -70° to -45°, β 130° to 230°, γ 40° to 50°, ϵ -170° to 20°, ζ -75° to -105°). Backbone torsions were left unrestrained for the metal-modified duplex **I-Ag** to allow the model freedom to explore possible alternative backbone conformations indicated by chemical shift changes in the ³¹P NMR spectrum.

Force-field parametrization. The X and Y building blocks were constructed using the RED server²⁸. To make fragments compatible with the standard library nucleotides, the Gaussian calculated electrostatic potentials output from the server were inputted again to the resp program (AmberTools 19) and the partial charges corresponding to the caps were kept constrained at the appropriate values.

MCPB.py was used to parametrize the metal-coordinated structures²³. The B3LYP functional with the DGDZVP basis set was used for the DFT calculations. Partial charges for the final fragments were refitted in Amber Tools using resp for compatibility.

Structure refinement. Starting structures were obtained through the fiber module of the NAB software, creating A-type and B-type Arnott DNA fibers. For duplexes **I** and **I-Ag** the standard nucleotides were appropriately substituted, and silver ions were inserted in place of the guanine H1 or thymine H3 protons to construct the starting silver-modified models.

Molecular dynamics simulations were performed with AMBER 20 software²⁹. The starting structures were subjected to a short minimization followed by a molecular dynamics run for a total duration of 60 ps (300,000 steps with a time step of 0.002 ns), during which the structures were heated to 400 K over 6 ps, kept at that temperature for 34 ps, then cooled to 0 K over the final 20 ps. Structures were checked for convergence. The ten lowest energy structures were selected for final analysis. DNA structure parameters were obtained from the web 3DNA server³⁰.

DFT calculations

Theoretical model was built using the Avogadro software^{31,32}. Sodium counterions were added to the phosphate groups, thus resulting in neutral model systems. Moreover, the solvent effect was included by the so-called explicit solvent model, in which 50 water molecules were placed around the molecule (base pairs, phosphates, counterions). After a partial geometry optimization of this model system, using semiempirical methods (PM3) within the ORCA 5.0.2 computational program^{33,34}, a suitable geometry was obtained for further complete optimization by quantum mechanics ab initio calculations using the PBEh-3c method³⁵. The latter method is a highly effective electronic structure technique that excels in optimizing geometries and calculating interaction energies of non-covalent complexes. This approach utilizes a global hybrid version of the Perdew-Burke-Ernzerhof (PBE) functional, which includes a significant proportion of non-local Fock-exchange (42%), and a valence-double-zeta Gaussian AO basis set (def2-mSVP) and Def2-ECP for silver³⁶. To correct for basis set

superposition errors (BSSE) and London dispersion effects, the gCP and D3 schemes are employed, respectively^{37,38}.

Data availability

Structure coordinates are deposited at the Protein Data Bank under accession code 9GDM (<https://www.rcsb.org/>), and data derived from NMR spectroscopy at the BioMagResBank under accession code 34942 (<https://bmr.io/>). The coordinates of the DFT-optimized structure generated in this study are provided in the Source Data file with this paper. All data were available from the corresponding authors upon request. Source data are provided with this paper.

References

1. Kallenbach, N. R., Ma, R. I. & Seeman, N. C. An immobile nucleic acid junction constructed from oligonucleotides. *Nature* **305**, 829–831 (1983).
2. Veneziano, R. et al. Designer nanoscale DNA assemblies programmed from the top down. *Science* **352**, 1534 (2016).
3. Ye, J. et al. Complex metal nanostructures with programmable shapes from simple DNA building blocks. *Adv. Mater.* **33**, e2100381 (2021).
4. Li, X. et al. DNA polyhedra with T-linkage. *ACS Nano* **6**, 5138–5142 (2012).
5. Huang, K. et al. Self-assembly of wireframe DNA nanostructures from junction motifs. *Angew. Chem. Int. Ed.* **58**, 12123–12127 (2019).
6. Chandrasekaran, A. R. & Levchenko, O. DNA nanocages. *Chem. Mater.* **28**, 5569–5581 (2016).
7. Rothmund, P. W. K. Folding DNA to create nanoscale shapes and patterns. *Nature* **440**, 297–302 (2006).
8. Chen, Z., Liu, C., Cao, F., Ren, J. & Qu, X. DNA metallization: principles, methods, structures, and applications. *Chem. Soc. Rev.* **47**, 4017–4072 (2018).
9. Al-Mahamad, L. L. G., El-Zubir, O., Smith, D. G., Horrocks, B. R. & Houlton, A. A coordination polymer for the site-specific integration of semiconducting sequences into DNA-based materials. *Nat. Commun.* **8**, 720 (2017).
10. Lippert, B. “Metal-modified base pairs” vs. “metal-mediated pairs of bases”: not just a semantic issue! *J. Biol. Inorg. Chem.* **27**, 215–219 (2022).
11. Naskar, S., Guha, R. & Müller, J. Metal-modified nucleic acids: metal-mediated base pairs, triples, and tetrads. *Angew. Chem. Int. Ed.* **59**, 1397–1406 (2020).
12. Müller, J. Nucleic acid duplexes with metal-mediated base pairs and their structures. *Coord. Chem. Rev.* **393**, 37–47 (2019).
13. Atsugi, T. et al. A novel Ag^I-DNA rod comprising a one-dimensional array of 11 silver ions within a double helical structure. *Angew. Chem. Int. Ed.* **61**, e202204798 (2022).
14. Kondo, J. et al. A metallo-DNA nanowire with uninterrupted one-dimensional silver array. *Nat. Chem.* **9**, 956–960 (2017).
15. Méndez-Arriaga, J. M., Maldonado, C. R., Dobado, J. A. & Galindo, M. A. Silver(I)-mediated base pairs in DNA sequences containing 7-deazaguanine/cytosine: towards DNA with entirely metallated Watson-Crick base pairs. *Chem. Eur. J.* **24**, 4583–4589 (2018).
16. Santamaría-Díaz, N., Méndez-Arriaga, J. M., Salas, J. M. & Galindo, M. A. Highly stable double-stranded DNA containing sequential silver(I)-mediated 7-deazaadenine/thymine Watson-crick base pairs. *Angew. Chem. Int. Ed.* **55**, 6170 (2016).
17. Megger, D. A. et al. Contiguous metal-mediated base pairs comprising two Ag(I) ions. *Chem. Eur. J.* **17**, 6533–6544 (2011).
18. Polonius, F.-A. & Müller, J. An artificial base pair, mediated by hydrogen bonding and metal-ion binding. *Angew. Chem. Int. Ed.* **46**, 5602–5604 (2007).
19. Ganguly, M. et al. A study of 7-deaza-2'-deoxyguanosine 2'-deoxycytidine base pairing in DNA. *Nucleic Acids Res.* **35**, 6181–6195 (2007).
20. Kowal, E. A. et al. Altering the electrostatic potential in the major groove: thermodynamic and structural characterization of 7-deaza-2'-deoxyadenosine:dT base pairing in DNA. *J. Phys. Chem. B* **115**, 13925–13934 (2011).
21. Swasey, S. M., Rosu, F., Copp, S. M., Gabelica, V. & Gwinn, E. G. Parallel guanine duplex and cytosine duplex DNA with uninterrupted spines of Ag^I-mediated base pairs. *J. Phys. Chem. Lett.* **9**, 6605–6610 (2018).
22. Swasey, S. M., Leal, L. E., Lopez-Acevedo, O., Pavlovich, J. & Gwinn, E. G. Silver (I) as DNA glue: Ag(+)-mediated guanine pairing revealed by removing Watson-Crick constraints. *Sci. Rep.* **5**, 10163 (2015).
23. Li, P. & Merz, K. M. Jr. MCPB.py: a Python based metal center parameter builder. *J. Chem. Inf. Model.* **56**, 599–604 (2016).
24. Schmidbaur, H. & Schier, A. Argentophilic interactions. *Angew. Chem. Int. Ed.* **54**, 746–784 (2015).
25. Johansen, S., Megger, N., Böhme, D., Sigel, R. K. O. & Müller, J. Solution structure of a DNA double helix with consecutive metal-mediated base pairs. *Nat. Chem.* **2**, 229–234 (2010).
26. Ilavsky, J. & Jemian, P. R. Irena: tool suite for modeling and analysis of small-angle scattering. *J. Appl. Crystallogr.* **42**, 347–353 (2009).
27. Zuo, X. et al. X-ray diffraction “fingerprinting” of DNA structure in solution for quantitative evaluation of molecular dynamics simulation. *Proc. Natl Acad. Sci. USA* **103**, 3534–3539 (2006).
28. Vanquelef, E. et al. R.E.D. Server: a web service for deriving RESP and ESP charges and building force field libraries for new molecules and molecular fragments. *Nucleic Acids Res.* **39**, W511–W517 (2011).
29. Case, D. A. et al. *Amber 2021* (Univ. California, 2021).
30. Li, S., Olson, W. K. & Lu, X.-J. Web 3DNA 2.0 for the analysis, visualization, and modeling of 3D nucleic acid structures. *Nucleic Acids Res.* **47**, W26–W34 (2019).
31. Avogadro: an open-source molecular builder and visualization tool. Version 1.2.0. <http://avogadro.cc/>.
32. Hanwell, M. D. et al. Avogadro: an advanced semantic chemical editor, visualization, and analysis platform. *J. Cheminform.* **4**, 17 (2012).
33. Neese, F. Software update: the ORCA program system, version 4.0. *Wiley Interdiscip. Rev. Comput. Mol. Sci.* **8**, e1327 (2018).
34. Neese, F. The ORCA program system. *Wiley Interdiscip. Rev. Comput. Mol. Sci.* **2**, 73–78 (2012).
35. Grimme, S., Brandenburg, J. G., Bannwarth, C. & Hansen, A. Consistent structures and interactions by density functional theory with small atomic orbital basis sets. *J. Chem. Phys.* **143**, 054107 (2015).
36. Andrae, D., Häußermann, U., Dolg, M., Stoll, H. & Preuß, H. Energy-adjusted ab initio pseudopotentials for the second and third row transition elements. *Theor. Chim. Acta* **77**, 123–141 (1990).
37. Grimme, S., Antony, J., Ehrlich, S. & Krieg, H. A consistent and accurate ab initio parametrization of density functional dispersion correction (DFT-D) for the 94 elements H–Pu. *J. Chem. Phys.* **132**, 154104 (2010).
38. Grimme, S., Ehrlich, S. & Goerigk, L. Effect of the damping function in dispersion corrected density functional theory. *J. Comput. Chem.* **32**, 1456–1465 (2011).

Acknowledgements

Financial support from Spanish MINECO (project PID2020-120186RB-I00), Spanish MICIU (Salvador Madariaga Program, Ref. PRX19/00290), Junta de Andalucía (project P20_00702). We also thank the “Centro de Servicios de Informática y Redes de Comunicaciones” (CSIRC) (UGR-Grid), Universidad de Granada, for providing computing time on the *Alhambra supercomputer*. U.J. and J.P. acknowledge the financial support of the Slovenian Research Agency (grants P1-0242 and J1-1704). O.P. acknowledges the financial support provided by the Spanish Ministerio de Ciencia e Innovación (PID2022-138479NB-I00). O.P. is member of the “Grup de Recerca de la Generalitat de Catalunya” (Ref. 2021 SGR 00668). We thank Matthew Cranswick, from the Advanced Technology

Manufacturing Institute at Oregon State University, for his support and assistance in conducting benchtop SAXS experiments (Anton Paar SAXSpace). The authors acknowledge the CERIC-ERIC Consortium for the access to experimental facilities and financial support (project 20172040 and 20222132). This research used the Advanced Photon Source (APS) resources, a US Department of Energy (DOE) Office of Science user facility operated for the DOE Office of Science by Argonne National Laboratory (ANL) under Contract No. DE-AC02-06CH11357. NSF's ChemMatCARS, Sector 15 at the APS, ANL, is supported by the Divisions of Chemistry (CHE) and Materials Research (DMR), National Science Foundation, under grant number NSF/CHE-1834750.

Author contributions

U.J. conducted and interpreted NMR experiments. A.P.-R contributed to experimental planning, and, together with C.L.-C, designed thermal-UV and CD experiments, executed and analyzed them. R.M.S. registered SAXS data. J.A.D. conceived, performed, and analyzed DFT calculations. O.P. recorded and analyzed MS experiments. M.N. and M.K.B. conceptualized SAXS and ASAXS experiments and analyzed the results. M.K.B. registered ASAXS data. J.P. conceived, designed the NMR experiments, and took the lead in solving the duplexes solution-state structures. M.A.G. recorded benchtop SAXS data, conceived the research idea, directed the research, and led manuscript writing. All authors provided essential input, shaping the research, analysis, and manuscript.

Competing interests

The authors declare no competing interests.

Additional information

Supplementary information The online version contains supplementary material available at <https://doi.org/10.1038/s41467-024-51876-8>.

Correspondence and requests for materials should be addressed to May Nyman, Janez Plavec or Miguel A. Galindo.

Peer review information *Nature Communications* thanks the anonymous reviewer(s) for their contribution to the peer review of this work. A peer review file is available.

Reprints and permissions information is available at <http://www.nature.com/reprints>

Publisher's note Springer Nature remains neutral with regard to jurisdictional claims in published maps and institutional affiliations.

Open Access This article is licensed under a Creative Commons Attribution-NonCommercial-NoDerivatives 4.0 International License, which permits any non-commercial use, sharing, distribution and reproduction in any medium or format, as long as you give appropriate credit to the original author(s) and the source, provide a link to the Creative Commons licence, and indicate if you modified the licensed material. You do not have permission under this licence to share adapted material derived from this article or parts of it. The images or other third party material in this article are included in the article's Creative Commons licence, unless indicated otherwise in a credit line to the material. If material is not included in the article's Creative Commons licence and your intended use is not permitted by statutory regulation or exceeds the permitted use, you will need to obtain permission directly from the copyright holder. To view a copy of this licence, visit <http://creativecommons.org/licenses/by-nc-nd/4.0/>.

© The Author(s) 2024